Catalyst discovery through megalibraries of nanomaterials

Edward J. Kluender[a,b,1], James L. Hedrick[b,c,1], Keith A. Brown[b,d], Rahul Rao[e,f], Brian Meckes[b,d], Jingshan S. Du[a,b], Liane M. Moreau[a,b], Benji Maruyama[e], and Chad A. Mirkin[a,b,c,d,2]

[a]Department of Materials Science and Engineering, Northwestern University, Evanston, IL 60208; [b]International Institute for Nanotechnology, Northwestern University, Evanston, IL 60208; [c]Department of Chemical and Biological Engineering, Northwestern University, Evanston, IL 60208; [d]Department of Chemistry, Northwestern University, Evanston, IL 60208; [e]Materials and Manufacturing Directorate, Air Force Research Laboratory, Wright–Patterson Air Force Base, OH 45433; and [f]UES Inc., Dayton, OH 45432

Edited by Catherine J. Murphy, University of Illinois at Urbana–Champaign, Urbana, IL, and approved November 20, 2018 (received for review September 6, 2018)

The nanomaterial landscape is so vast that a high-throughput combinatorial approach is required to understand structure–function relationships. To address this challenge, an approach for the synthesis and screening of megalibraries of unique nanoscale features (>10,000,000) with tailorable location, size, and composition has been developed. Polymer pen lithography, a parallel lithographic technique, is combined with an ink spray-coating method to create pen arrays, where each pen has a different but deliberately chosen quantity and composition of ink. With this technique, gradients of Au-Cu bimetallic nanoparticles have been synthesized and then screened for activity by in situ Raman spectroscopy with respect to single-walled carbon nanotube (SWNT) growth. Au_3Cu, a composition not previously known to catalyze SWNT growth, has been identified as the most active composition.

combinatorial screening | catalysis | multimetallic nanoparticle synthesis | carbon nanotube growth | in situ Raman spectroscopy

High-throughput screening is a valuable tool for facilitating rapid scientific discovery in many fields (1–3). Such approaches enable the ability to synthesize combinatorial libraries and subsequently probe numerous reaction conditions, which allows for the identification of structures with unusual and in certain cases, useful properties. Consequently, combinatorial libraries have been utilized in diverse fields spanning catalysis, drug discovery, and basic cell biology (4–15). Indeed, high-throughput techniques have contributed to a disruptive shift in scientific discovery.

By applying the same principles learned from the field of biology to the materials discovery space, one can take a similar approach to explore the materials genome. Previously, high-throughput studies of solid-state materials have investigated the properties of bulk materials and thin films down to the micrometer scale (16–23) but have not reached the nanoscale, where the properties of materials begin to significantly change (24). However, as one transitions from the microscale to the nanoscale, the synthesis challenge increases exponentially, since it becomes necessary to control size and composition with nanometer precision. In addition, the number of possibilities that need to be evaluated also dramatically increases, as one can examine particles at a fixed compositional ratio that vary in size, atomic distribution, and structure. With the advent of polymer pen lithography (PPL) (25), a massively parallel cantilever-free scanning probe methodology, and scanning probe block copolymer lithography (SPBCL) (26–28), a technique that utilizes patterned nanoreactors composed of block copolymers coordinated to metal precursors to form single nanoparticles in each nanoreactor, one can fabricate arrays of >5 billion individual site-isolated, compositionally identical, and size-uniform nanoparticles that are spatially encoded on a chip (29). From this perspective, a major advance would be to develop methodology for making complex megalibraries that consist of compositionally distinct particles, each of which, in principle, is capable of displaying unique chemical and physical properties. Moreover, for such libraries to be useful, ways of screening them are essential.

Herein, we report a platform for the synthesis and screening of combinatorial libraries of chemically distinct multimetallic nanoparticles for their ability to catalyze the growth of carbon nanotubes (CNTs), specifically single-walled carbon nanotubes (SWNTs); these are a unique class of materials that have been at the forefront of nanotechnology for the past two decades but with large-scale applicability that has been hindered by the inability to grow them with defined structures and properties (30). To accomplish this, we paired our nanoparticle synthesis method with a high-throughput automated system for growing and monitoring SWNTs in real time using in situ Raman spectroscopy. First, we describe a spray-coating method for inking PPL pen arrays with linear gradients of ink compositions (Fig. 1 *A*–*C*). Second, we describe how an Autonomous Research System (ARES) (31–34) can be used to rapidly synthesize SWNTs from the potential catalyst nanoparticles and screen the products by Raman spectroscopy to determine which composition exhibits the greatest yield of SWNTs under a well-defined set of conditions (Fig. 1*D*). Using these techniques to study gradients of Au-Cu alloy nanoparticles, we have discovered that the Au_3Cu composition exhibits the highest catalytic activity for SWNT growth. To our knowledge, this composition of nanoparticle has never been identified as a

Significance

Discovering new materials is traditionally a slow process, as the materials genome encompasses a massive parameter space, particularly on the nanoscale where synthesis methods are less universal. To overcome this challenge, a cantilever-free lithography method has been used to deposit millions of discrete nanoreactors on a substrate, which can be transformed into millions of nanoparticles spatially encoded in terms of composition and size. These compositions were screened for their ability to catalytically grow carbon nanotubes, and a composition (Au_3Cu) was identified as optimum for this application. More generally, this combinatorial method of synthesizing nanoparticle megalibraries offers researchers a platform for identifying structures with desired properties at a rate not previously possible.

Author contributions: E.J.K., J.L.H., K.A.B., R.R., B. Maruyama, and C.A.M. designed research; E.J.K., J.L.H., R.R., B. Meckes, J.S.D., and L.M.M. performed research; E.J.K., J.L.H., K.A.B., R.R., B. Meckes, J.S.D., and L.M.M. analyzed data; and E.J.K., J.L.H., and C.A.M. wrote the paper.

Conflict of interest statement: K.A.B. and C.A.M. have financial interests in TERA-print, LLC, which could potentially benefit from the outcomes of this research. All other authors declare no competing interests.

This article is a PNAS Direct Submission.

[1]E.J.K. and J.L.H. contributed equally to this work.

[2]To whom correspondence should be addressed. Email: chadnano@northwestern.edu.

This article contains supporting information online at www.pnas.org/lookup/suppl/doi:10.1073/pnas.1815358116/-/DCSupplemental.

Published online December 17, 2018.

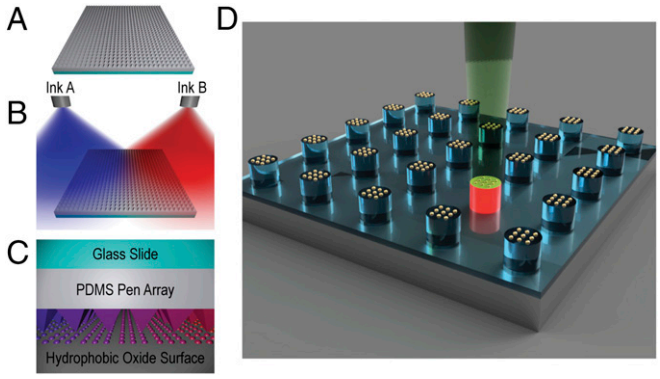

Fig. 1. Spray-coating process for generating combinatorial libraries and ARES SWNT growth. (*A*) PPL array, made of polydimethylsiloxane (PDMS) on a glass slide, before inking, (*B*) dual spray coating of two different inks onto the PPL array to make compositional gradients, and (*C*) patterning combinatorial libraries of nanomaterials by mounting the PPL array on a piezo scanner. (*D*) Schematic of the ARES setup for laser-induced CVD growth of SWNTs from metal nanoparticles on Si micropillars patterned using PPL.

catalyst for SWNT growth. Finally, it is important to note that, although this is an initial proof-of-concept demonstration of how megalibraries can be used to study vast size and compositional spaces, the implications of the study and results extend way beyond the discovery of catalysts for SWNT growth and the tool (Raman spectroscopy) used to interrogate the library.

Results and Discussion

Nanopatterning Compositional Gradients over Large Areas. To explore the combination of PPL with pen array spray coating as a method for generating combinatorial libraries, the radial distribution of ink deposition was evaluated by performing a spray-coating operation on a target substrate held at various distances from the nozzle. Quantitative evaluation of this distribution was done by imaging the substrate and examining the intensity of the image in a line across the center of the image (*SI Appendix*, Fig. S1*B*). When the intensity profile was fit to a Gaussian function, there was a nearly linear section from 0.15 to 0.85 of normalized intensity (*SI Appendix*, Fig. S1 *C* and *D*). To increase capabilities, a second spray gun was utilized to create overlapping profiles that result in a combinatorial gradient that can be reliably modeled (*SI Appendix*, Fig. S1*A*). Utilizing the relationship between the linear region of the sprayed surface and the nozzle–sample distance, we found that inking a typical 1.5-cm-wide PPL pen array with a gradient that varies from ∼15–85% requires two spray guns with a separation of 5 cm that are positioned 20 cm from the pen array.

To evaluate the potential for reliably transferring the gradient formed on the PPL array to an underlying substrate (Si/SiO_2), two aqueous inks, consisting of rhodamine 6G or sulfo-cyanine5 NHS ester in poly(ethylene oxide)-*b*-poly(2-vinylpyridine) (PEO-*b*-P2VP), were prepared and studied. These dyes were chosen, because they can be spectrally distinguished by fluorescence microscopy. The inking procedure consisted of simultaneously spraying the two inks, each aimed at the center of opposing edges of the PPL pen array, and then allowing the solutions to completely dry before patterning (*SI Appendix*, Fig. S2*D*). During the drying process, the ink deposited onto the array mixes between neighboring pens, but the ink dries around the base of the pens before global mixing occurs (*SI Appendix*, Fig. S3). After drying, a gradient could be seen by eye across the PPL array (*SI Appendix*, Fig. S4*A*). To characterize the gradient, the whole PPL array was imaged utilizing a confocal microscope. To maintain high resolution to visualize the nanoscale features across the whole array, thousands of images were taken on two tracks, one for each fluorophore, and they were subsequently stitched and stacked to make a single image with 268 million pixels (*SI Appendix*, Fig. S4*B*). To verify that spray-coated PPL pen arrays can be used to pattern surfaces with the same compositional gradient, the dual spray-coated PPL array was used to print polymer dots onto a hexamethyldisilazane (HMDS)-treated silicon substrate that was imaged in the same way as the array (*SI Appendix*, Fig. S2 *A* and *C*). The counter propagating changes in fluorescence contrast indicate that the spray coating was effective and created a red–blue, left-to-right gradient. To quantify the distribution of the ink, the image stacks were averaged to construct a profile plot of fluorescence intensity (*SI Appendix*, Fig. S2*B*). The fluorescence intensity plots demonstrate the potential for dual spray coating to generate near linear gradients of ink composition on PPL pen arrays.

Nanopatterning Composition and Size Dual Gradients. While the ability to generate patterns with compositional gradients on the nanoscale is potentially useful, realizing combinatorial patterns with control over the size and composition of every feature in the pattern is the ultimate goal for high-throughput screening. In addition to inking the pen arrays with uniform quantities of ink while varying their composition, it is possible to vary the quantity of ink on each pen as a means to change the rate of ink deposition. It is important to note that, while similar linear gradients have been previously achieved by patterning with pen arrays that have been deliberately tilted to change pen–sample contact area or contact time across the array, controlling feature size with ink loading affords the option of realizing nonlinear gradients in patterned feature size (35, 36). To explore the ability of spray coating to generate such combinatorial libraries, a dual spray-coating experiment was performed in which the two airbrushes were loaded with the same polymer–fluorophore inks as previously used but were aimed above two adjacent corners of the pen array (rather than along a line that passes through the center of the array) (Fig. 2*E* and *SI Appendix*, Fig. S5). Subsequently, PPL was performed with each pen in the array being used to print a 30 × 30 array of dot features (Fig. 2*D*). Given that this 126 × 126 pen array contained 15,876 pens, the final pattern was composed of over 14 million discrete polymer features. To characterize this massive array of features, large-scale fluorescence images were acquired, which clearly showed a macroscopic gradient in fluorescence across the patterned surface (Fig. 2*A*). Indeed, the average fluorescence intensity is well described by a linear gradient across the entire patterned surface horizontally (Fig. 2*B*). Also, fluorescence intensity and atomic force microscopy (AFM) data show a nonlinear size gradient of features ranging from 1.10 ± 0.02 μm to 642 ± 46 nm in diameter and from 17 ± 1 to 3.6 ± 0.8 attoliters in volume going from the top of the array to the bottom (Fig. 2 *C*, *F*, and *G*).

Nanoparticle Compositional Gradient Patterned onto the ARES Micropillars. While prior experiments focused on patterning gradients with easy to detect fluorophores to visualize and characterize the gradients, it is important to validate that combinatorial libraries may be generated using substances where the function can, in principle, dramatically change across the array. When combined with SPBCL, catalytically active (vide infra) multimetallic nanoparticles with gradients of composition can be readily synthesized. To determine if combining SPBCL and dual spray coating can be used to generate compositional gradients, we explored the patterning of metal ion-loaded block copolymers that can be compositionally quantified using X-ray fluorescence (XRF) (37). To explore the patterning of these inks, a pen array was dual spray coated using aqueous solutions of PEO-*b*-P2VP: one with auric acid and the other with sodium tetrachloropalladate. After spray coating, this pen array was used to pattern features on an HMDS-treated silicon wafer. The resulting features were heat treated to form nanoparticles and were characterized using XRF, which allowed for the calculation of the local atomic ratio of Au to Pd in sections across the array (*SI Appendix*, Figs. S6 and S7). As expected, the atomic ratio of Au to total Au and Pd varied from 9 to 88%. Pd was used for this analysis as opposed to Cu, which is

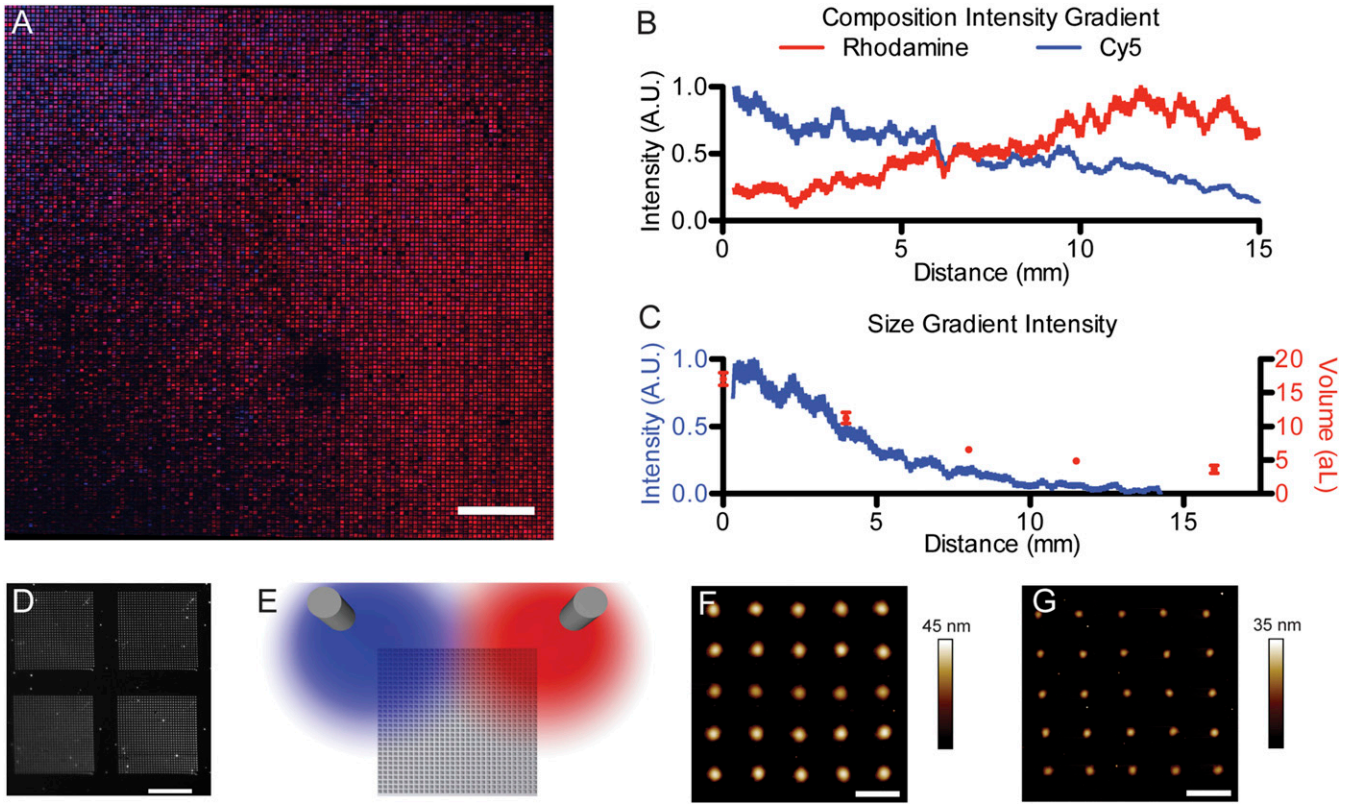

Fig. 2. Large-scale nanopatterned gradients of composition and size. (*A*) Stitched confocal fluorescence image of compositional and size gradients of two fluorophores in polymeric domes. (Scale bar: 2 mm.) (*B*) Average fluorescence intensity of each fluorophore across the array and (*C*) average total fluorescence intensity (blue curve) in the vertical axis plotted with the average volume of individual features as measured by AFM (red dots; error bars represent SD). (*D*) High-resolution dark-field micrograph of a region showing the patterns written by four pens. (Scale bar: 50 μm.) (*E*) Schematic of the airbrush position during spraying. (*F*) AFM of the largest patterned features (1.10 ± 0.02 μm) at the top of the array and (*G*) AFM of the smallest patterned features (642 ± 46 nm) at the bottom of the array. (Scale bars: 3 μm.)

studied later, due to the larger signal separation from Au in the XRF spectrum.

Equally important to synthesizing these centimeter-scale continuous compositional gradients is developing methods to measure the properties of the resulting nanoparticles. The property measured here is the nanoparticle's ability to catalyze the growth of SWNTs by laser-induced chemical vapor deposition (CVD). This is performed in ARES, which utilizes substrates containing thousands of thermally isolated silicon micropillars (10-μm diameter and height) that are instantaneously heated to SWNT growth temperatures (700 °C to 900 °C) using a high-power visible laser (532 nm, 6 W maximum power) inside a vacuum chamber containing a reducing agent (H_2) and a hydrocarbon source (C_2H_4). This heating laser is also used as the excitation laser for measuring the Raman peaks from the growing SWNTs, namely the low-frequency, diameter-dependent (between 100 and 300 cm^{-1}, corresponding to SWNT diameters ranging from ∼0.8 to 2.5 nm) radial breathing modes, the disorder-induced D band (at ∼1,350 cm^{-1}), and the graphitic G band (at ∼1,590 cm^{-1}). Each ARES substrate is 5 × 5 mm^2 in dimension and contains a 12 × 12 array of numbered patches spaced 400 μm apart, each consisting of a 5 × 5 array of 10-μm-diameter pillars spaced 50 μm apart. A polymer pen array was fabricated with 15-μm-base length pyramidal pens with the same spacing as the pillars on an ARES substrate. Using a rotational stage and a three-axis piezo actuator to align the pen array with the substrate (Fig. 3*A*), attoliter polymer domes with metal precursor containing PEO-*b*-P2VP ink were deposited in an ordered array on top of HMDS-treated micropillars (Fig. 3*B*). Following a three-step heat treatment (precursor aggregation, particle formation, and calcination), catalytically active particles were synthesized on top of the 3,600 micropillars, allowing for high-throughput SWNT growth and in situ characterization.

CNT Growth from Au_XCu_{1-X} Nanoparticles. To analyze the catalytic activity of the Au_XCu_{1-X} system, a 1.5-cm-wide pen array was spray coated with solutions containing auric acid and cupric nitrate. The compositional gradient was deliberately varied from X = 0.12 to X = 0.85, calculated using the Gaussian spray profiles. While transition metal catalysts, like Fe and Co, are traditionally used for SWNT growth, recent breakthroughs using bimetallic catalysts, such as W-Co (38), prompted us to study an alloy system for this application, Au-Cu, which is known to form fully miscible phases at the nanoscale over all compositions (28, 39). Both elements—Au and Cu—have been used for SWNT growth as monometallic particles (40, 41). For this initial proof-of-concept catalyst screen, we chose to only study particle composition effects on SWNT growth. Due to the size restriction (1–3 nm) of catalytically active particles for SWNT growth, a size gradient was not included in this screen. The nanoparticles used in SWNT growths were ∼2.5 nm in size (*SI Appendix*, Fig. S8) and are composed of Au and Cu uniformly mixed at the nanometer scale (*SI Appendix*, Fig. S9). When particles are larger than this size regime, multiwalled CNTs are the primary product (*SI Appendix*, Fig. S10).

The 5-mm width of the ARES substrate requires the 1.5-cm gradient to be split evenly into three sections. Each section was patterned onto a separate substrate, resulting in three gradients with ∼24% composition change. Across an ARES substrate, there are 12 columns of patches; assuming that the variation of final particle composition has a distribution of roughly 5%, each vertical column of patches can be treated as a single composition,

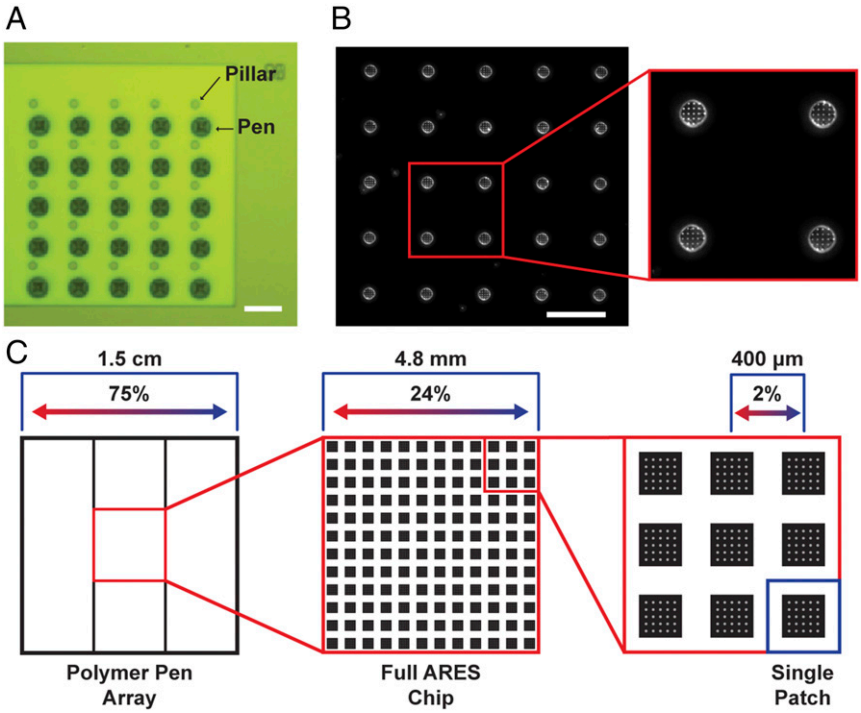

Fig. 3. Patterning compositional nanoparticle gradients onto ARES micropillars. (*A*) Image of the pen arrays aligned with the ARES micropillars. (Scale bar: 50 μm.) (*B*) Dark-field optical image. (Scale bar: 50 μm.) (*Inset*) Four pillars with the nanodome polymer features in a square array on top of the micropillars. (Magnification: 2.2×.) (*C*) Compositional breakdown of 75% composition gradient across three 5-mm micropillar substrates.

with a 2% composition change from column to column (Fig. 3*C*). We know that this is accurate, because the tight correlation between ink composition and resulting particle composition has been studied in detail (27, 28). All three substrates were heat treated to form catalytically active particles and placed into the ARES reaction chamber. Growths were performed in two temperature ranges: from 700 °C to 800 °C and from 800 °C to 900 °C. Each pillar was individually heated to the growth temperature under a total pressure of 20 torr, consisting of C_2H_4 (partial pressure 13.5 torr) and H_2 (6.5 torr). SWNT growth occurred over 1 min. After each growth, the laser power was turned down, and a low-power 30-s Raman scan was collected at room temperature. The integrated intensity of the G band, normalized to the Si peak, from this room temperature scan (G_{max}) is proportional to the yield of the SWNTs on the micropillar. Ten growths were performed for each nanoparticle composition (five in each temperature range), amounting to a total of 360 growth experiments.

The average G_{max} values are shown as a function of nanoparticle composition in Fig. 4*A*, visualizing the growths performed at 700 °C to 800 °C. Representative Raman spectra in the G-band region of the SWNTs are shown for five different alloy compositions in Fig. 4*B*. Growths performed between 800 °C and 900 °C are shown in *SI Appendix*, Fig. S11. The largest increase in catalytic activity was observed at X = 0.75. While this composition was not previously known for its ability to catalyze SWNT growth, it has been shown to have enhanced catalytic activity in electrochemistry, with Au_3Cu exhibiting a peak activity for the reduction of CO_2 greater than any other composition in the Au-Cu system (42). Moreover, we observed higher overall SWNT yield in the lower-temperature range. Taking melting point depression into account, these growth temperatures are near the melting points of Au-Cu nanoalloys, with particles containing a higher gold content having higher melting temperatures (39). Thus, our lower (700 °C to 800 °C) and higher (800 °C to 900 °C) growth temperatures may correspond to solid and liquid catalysts, respectively. In addition to the in situ data, diameter-dependent radial breathing modes were collected using ex situ Raman spectroscopy, which indicate increasing SWNT diameters with Au fraction (*SI Appendix*, Fig. S12).

Our observation of enhanced catalytic activity at Au_3Cu is not limited to the ARES experiments. We independently confirmed the ARES results with more traditional tube furnace-based thermal CVD growth experiments, where the appropriate amounts of Au and Cu were used in the form of salts (auric acid and cupric nitrate) dissolved in ethanol followed by dip coating of SiO_2 substrates. Samples were made at compositions of X = 0, 30, 50, 70, and 100. While the products from these growths exhibited a higher D-band intensity due to an excess of ethylene being present (the tube furnace growths were performed at atmospheric pressure, while ARES growths were carried out at 20 torr; excess ethylene leads to more disordered C), the G-band trends for the growths performed with the SPBCL-synthesized particles were mirrored using this more conventional particle synthesis and growth method (*SI Appendix*, Fig. S13).

Conclusion

In conclusion, we have reported a method for rapidly synthesizing and screening massively complex combinatorial megalibraries of nanostructures. These greater than 1-million particle libraries are the first of their kind and lay the foundation for a type of inorganic combinatorial science that focuses on using such libraries to identify properties associated with nanostructures of interest. These libraries contain approximately as many new inorganic materials as scientists have cumulatively made to date. The ability to generate megalibraries of polyelemental nanoparticles will allow researchers to ask and answer key questions in fields beyond catalysis, including photonics, plasmonics, magnetism, solar light harvesting, biology, and nanomedicine. Moreover, this synthetic capability will challenge researchers in these fields to develop rapid ways of probing discrete locations of the libraries to screen for properties of interest, which may dramatically vary from system to system.

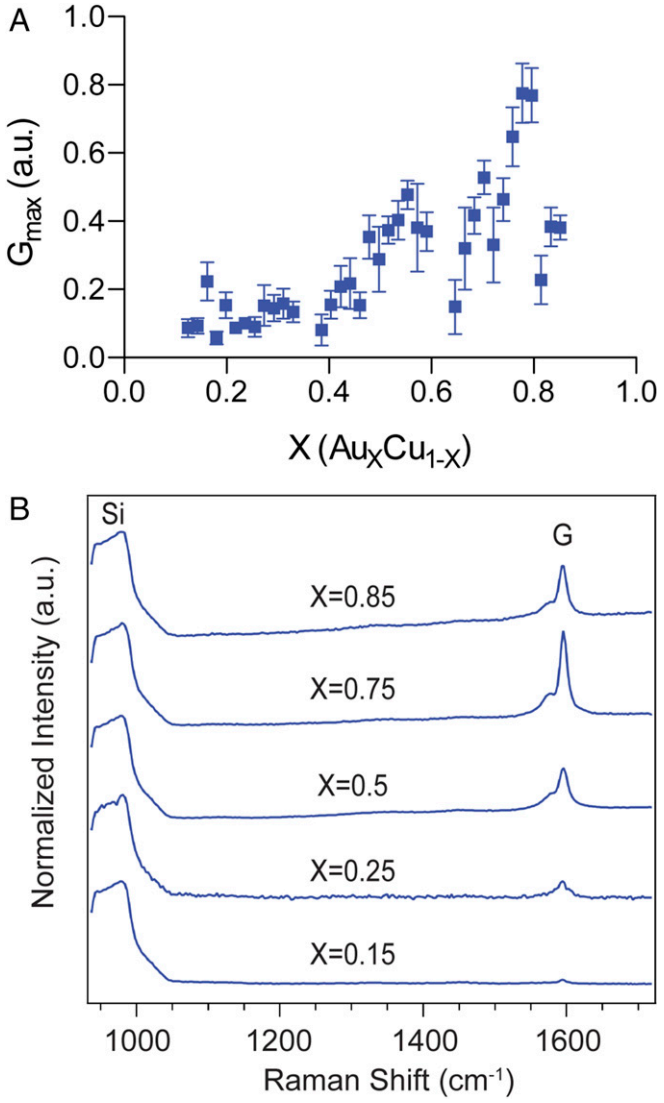

Fig. 4. Compositional breakdown of catalytic activity. (*A*) Integrated intensity of the SWNT Raman G band as a function of catalyst composition for growths performed between 700 °C and 800 °C. Error bars represent SEM. Growths performed between 800 °C and 900 °C are plotted in *SI Appendix*, Fig. S11. The G_{max} peaks around X = 0.75, suggesting Au_3Cu as the composition that exhibits the highest catalytic activity for SWNT growth. (*B*) Representative Raman spectra from growths on ARES micropillars at five compositions normalized to the Si peak.

Experimental Procedures

Materials. Polydimethylsiloxane was made from 3.4 g of vinyl compound-rich prepolymer (VDT-731) and 1.0 g of hydrosilane-rich cross-linker (HMS-301) with 20 (wt/wt) ppm of platinum-divinyltetramethyldisiloxane complex in xylene (SIP 6831.1) from Gelest as well as 0.1% (wt/wt) 2,4,6,8-tetramethyltetravinylcyclotetrasiloxane from Fluka. HMDS and rhodamine 6G were obtained from Sigma-Aldrich. PEO-*b*-P2VP (Mn = 2.8-*b*-1.5 kg·mol^{-1}) was obtained from Polymer Source. Glass slides were obtained from VWR. Sulfo-cyanine5 NHS ester was obtained from Lumiprobe Corporation. Metal compounds, auric acid, sodium tetrachloropalladate, and cupric nitrate were purchased from Sigma-Aldrich and used without additional purification. Harder Steenbeck Infinity 2 in 1 CR plus airbrush with Harder Steenbeck fine pressure valve and Iwata Power Jet Pro IS-975 Dual Piston Compressor were obtained from Chicago Air Supply; 4-inch P doped silicon oxide wafers were obtained from Nova Electronic Materials.

Pen Array Fabrication. PPL arrays were made as previously reported (25, 43).

Ink Preparation. Fluorophore-containing inks were aqueous solutions composed of 5 mg/mL of PEO-*b*-P2VP along with 10 mg/mL of a fluorophore (either rhodamine 6G or sulfo-cyanine5 NHS ester). Solutions with fluorophore compounds were wrapped in foil and kept on a shaker for 1 h. Inks for metal nanoparticle synthesis were composed of 5 mg/mL of PEO-*b*-P2VP and a concentration of metal precursors with a molar ratio of pyridine groups to metal atoms ranging from 64 (XRF measurements) to 256 (SWNT growths). Solutions containing metal precursors were brought to pH values of three to four and shaken for 12–24 h.

Spray Coating. All pen arrays were plasma cleaned for 2 min under oxygen at 60 W before spray inking. The ink solutions (150 μL per gun) were spray coated onto the array using 0.15-mm needles at 20 psi airflow using Harder Steenbeck Infinity CR plus airbrushes with an Iwata Power Jet Pro IS-975 dual piston compressor. The two airbrushes were sprayed in unison. After spraying, the pen arrays were placed with the pens facing up and covered for 15 min while the solution dried. Custom airbrush holders were designed on TinkerCad, rendered in Slic3r, and 3D printed out of acrylonitrile butadiene styrene using a SeeMeCNC Orion Delta 3D printer.

Substrate Preparation. Silicon wafers and ARES micropillar substrates were vapor coated in a desiccator for 24 h with HMDS in hexane to render them hydrophobic.

Patterning. Patterning was performed using a Park XE-150 in a humidity control chamber at a relative humidity between 70 and 95% and at room temperature with a 30-min incubation period before patterning.

Nanoparticle Synthesis. To convert polymer features into nanoparticles, the substrates were put into a tube furnace and thermally annealed. The heating conditions were as follows. The furnace was ramped to 120 °C to 240 °C (this temperature is below the decomposition temperature of the polymer) under Ar atmosphere, held at this temperature for 20–48 h, and then cooled back to room temperature. The atmosphere was switched to H_2; the temperature was then ramped to 500 °C in 2 h, held at 500 °C for 8–12 h, and finally cooled down to room temperature. The metal precursors aggregate during the first step under Ar followed by nanoparticle formation and reduction during the second step under H_2. For SWNT catalyst particle preparation, an additional calcination step was performed in air.

Imaging. AFM measurements were performed on a Dimension Icon (Bruker) to obtain 3D profiles of the patterns. Images were processed in Nanoscope Analysis 1.5. Confocal images were taken with a Zeiss LSM 800 Confocal Microscope. Images were processed with ImageJ and Zen Blue. Maximum intensity projections of confocal stacks were generated for each tile. Tiles were stitched with vignette corrections. Intensity plots were created from 500-pixel moving averages.

XRF. Data were collected at sector 5 bending magnet D branch beamline (beamline 5-BM-D) of the Advanced Photon Source. Fluorescence spectra were collected at an incident energy of 24.8 keV using two four-element Vortex ME-4 silicon drift diode detectors. The sample was placed in a glancing incidence geometry with respect to the X-ray beam at an angle of ∼0.1°. A horizontal slit size of 3 mm was used, and the sample was translated to probe the Au-Pd gradient at various points on the sample. The vertical slit size was adjusted according to footprint calculation, such that the entire sample length would be measured, to both maximize fluorescence counts from the elements of interest and achieve a global representation of the Au-Pd gradient.

Scanning Transmission Electron Microscopy. Polymer nanoreactors containing Au and Cu precursor ions were deposited on 15-nm silicon nitride membranes using dip pen nanolithography and thermally treated under the same conditions as described earlier. Scanning transmission electron microscopy imaging was performed on a JEOL ARM200 equipped with a CEOS probe corrector and dual energy-dispersive X-ray spectroscopy detectors. The high-angle annular dark-field images were collected with a collection angle of 68–280 mrad, and annular bright-field images were collected with a collection angle of 8–34 mrad.

SWNT Growth in ARES Micropillars. To write the particles onto the micropillar substrates used for ARES, a rotational stage was integrated into the patterning stage to allow for the alignment of pens with pillars. Nanoparticles were synthesized on the pillars. Before being placed into the ARES growth chamber, the substrate with micropillars was calcinated at 600 °C under air

for 10 min to remove residual carbon from the nanoparticles. After loading the substrate into the ARES chamber, it was pumped down to a base pressure of ~1E−6 torr overnight followed by backfilling the chamber to the growth pressure (20–50 torr containing varying partial pressures of C_2H_4 and H_2). Using a 532-nm laser as both a heating source and a Raman excitation laser, the 10-μm pillar was heated to the growth temperature under the growth atmosphere to initiate SWNT growth. The micropillar temperature was estimated from the frequency shifts of the Si peak, based on literature reports (33, 34). After growth, the integrated intensity (normalized to the Si peak) of the G band was calculated as a measure of the total SWNT yield. Additional Raman spectra were also collected ex situ using a standard Raman microscope (Renishaw InVia; 514.5-nm excitation).

Screening Platform Work Flow. Polymer pen arrays were made using Si masters, which contained pyramidal pits with a pitch and density to align with ARES substrates. Au- and Cu-containing polymer solutions were prepared and shaken overnight. Concurrently, the ARES substrates were treated with HMDS to make them more hydrophobic. The next morning, the pen array was spray coated with the Au-Cu composition gradient and used to pattern polymer domes onto the micropillars. That night, the substrates were loaded into a tube furnace under an Ar atmosphere and stepwise heat treated to form a bimetallic nanoparticle in each polymer dome. Before being loaded into the ARES vacuum chamber, a calcination was performed under air in a tube furnace to remove any residual carbon resulting from decomposition of the polymer dome. The growth gases were back filled into the ARES vacuum chamber and allowed to equilibrate. Growths were performed at two temperatures across the entire gradient over 3 d (1 d for each substrate). The in situ Raman spectra were analyzed using peak integration calculations. From start to finish, the megalibrary screening platform allowed for comprehensive combinatorial screening of multimetallic nanoparticles in 5–6 d.

ACKNOWLEDGMENTS. This material is based on work supported by the Sherman Fairchild Foundation, Inc.; Air Force Office of Scientific Research Award FA9550-16-1-0150; Air Force Research Laboratory Agreement FA8650-15-2-5518; and Air Force Office of Scientific Research Laboratory Research Independent Research Grant 16XCOR322. Research reported in this publication was also supported by National Cancer Institute of the NIH Award U54CA199091. We acknowledge additional support from the Vannevar Bush Faculty Fellowship Program sponsored by the Basic Research Office of the Assistant Secretary of Defense for Research and Engineering and funded by Office of Naval Research Grant N00014-15-1-0043. J.L.H. and L.M.M. acknowledge support from the Department of Defense through the National Defense Science & Engineering Graduate Fellowship Program. This work utilized the Northwestern University Micro/Nano Fabrication Facility and the Electron Probe Instrumentation Center Facilities of the Northwestern University Atom and Nanoscale Chacterization Experimental Center, which are partially supported by Soft and Hybrid Nanotechnology Experimental Resource NSF Grant ECCS-1542205, Materials Research Science and Engineering Center Grant DMR-1720139, and the State of Illinois. The US Government is authorized to reproduce and distribute reprints for governmental purposes notwithstanding any copyright notation thereon.

1. Mayr LM, Bojanic D (2009) Novel trends in high-throughput screening. *Curr Opin Pharmacol* 9:580–588.
2. Fonseca MH, List B (2004) Combinatorial chemistry and high-throughput screening for the discovery of organocatalysts. *Curr Opin Chem Biol* 8:319–326.
3. Weidenhof B, et al. (2009) High-throughput screening of nanoparticle catalysts made by flame spray pyrolysis as hydrocarbon/NO oxidation catalysts. *J Am Chem Soc* 131: 9207–9219.
4. Al-Lazikani B, Banerji U, Workman P (2012) Combinatorial drug therapy for cancer in the post-genomic era. *Nat Biotechnol* 30:679–692.
5. Basabe-Desmonts L, Reinhoudt DN, Crego-Calama M (2006) Combinatorial fabrication of fluorescent patterns with metal ions using soft lithography. *Adv Mater* 18: 1028–1032.
6. Battersby BJ, Trau M (2002) Novel miniaturized systems in high-throughput screening. *Trends Biotechnol* 20:167–173.
7. Bunin BA, Plunkett MJ, Ellman JA (1994) The combinatorial synthesis and chemical and biological evaluation of a 1,4-benzodiazepine library. *Proc Natl Acad Sci USA* 91: 4708–4712.
8. Clark MA, et al. (2009) Design, synthesis and selection of DNA-encoded small-molecule libraries. *Nat Chem Biol* 5:647–654.
9. Hertzberg RP, Pope AJ (2000) High-throughput screening: New technology for the 21st century. *Curr Opin Chem Biol* 4:445–451.
10. Jiang X, et al. (2005) A general method for patterning gradients of biomolecules on surfaces using microfluidic networks. *Anal Chem* 77:2338–2347.
11. Khandurina J, Guttman A (2002) Microchip-based high-throughput screening analysis of combinatorial libraries. *Curr Opin Chem Biol* 6:359–366.
12. MacBeath G, Schreiber SL (2000) Printing proteins as microarrays for high-throughput function determination. *Science* 289:1760–1763.
13. Mei Y, et al. (2010) Combinatorial development of biomaterials for clonal growth of human pluripotent stem cells. *Nat Mater* 9:768–778.
14. Ricoult SG, Kennedy TE, Juncker D (2015) Substrate-bound protein gradients to study haptotaxis. *Front Bioeng Biotechnol* 3:40.
15. Zimmermann G, Neri D (2016) DNA-encoded chemical libraries: Foundations and applications in lead discovery. *Drug Discov Today* 21:1828–1834.
16. Maier WF, Stöwe K, Sieg S (2007) Combinatorial and high-throughput materials science. *Angew Chem Int Ed Engl* 46:6016–6067.
17. Hattrick-Simpers J, Wen C, Lauterbach J (2015) The materials super highway: Integrating high-throughput experimentation into mapping the catalysis materials genome. *Catal Lett* 145:290–298.
18. Senkan S (2001) Combinatorial heterogeneous catalysis-A new path in an old field. *Angew Chem Int Ed Engl* 40:312–329.
19. Xiang X-D, et al. (1995) A combinatorial approach to materials discovery. *Science* 268: 1738–1740.
20. Briceño G, Chang H, Sun X, Schultz PG, Xiang X-D (1995) A class of cobalt oxide magnetoresistance materials discovered with combinatorial synthesis. *Science* 270: 273–275.
21. Danielson E, et al. (1997) A combinatorial approach to the discovery and optimization of luminescent materials. *Nature* 389:944–948.
22. Reddington E, et al. (1998) Combinatorial electrochemistry: A highly parallel, optical screening method for discovery of better electrocatalysts. *Science* 280:1735–1737.
23. Potyrailo R, et al. (2011) Combinatorial and high-throughput screening of materials libraries: Review of state of the art. *ACS Comb Sci* 13:579–633.
24. Ferrando R, Jellinek J, Johnston RL (2008) Nanoalloys: From theory to applications of alloy clusters and nanoparticles. *Chem Rev* 108:845–910.
25. Huo F, et al. (2008) Polymer pen lithography. *Science* 321:1658–1660.
26. Chai J, et al. (2010) Scanning probe block copolymer lithography. *Proc Natl Acad Sci USA* 107:20202–20206.
27. Chen P-C, et al. (2015) Tip-directed synthesis of multimetallic nanoparticles. *J Am Chem Soc* 137:9167–9173.
28. Chen P-C, et al. (2016) Polyelemental nanoparticle libraries. *Science* 352:1565–1569.
29. Hedrick JL, et al. (2016) Hard transparent arrays for polymer pen lithography. *ACS Nano* 10:3144–3148.
30. De Volder MFL, Tawfick SH, Baughman RH, Hart AJ (2013) Carbon nanotubes: Present and future commercial applications. *Science* 339:535–539.
31. Rao R, Liptak D, Cherukuri T, Yakobson BI, Maruyama B (2012) In situ evidence for chirality-dependent growth rates of individual carbon nanotubes. *Nat Mater* 11: 213–216.
32. Rao R, et al. (2013) Revealing the impact of catalyst phase transition on carbon nanotube growth by in situ Raman spectroscopy. *ACS Nano* 7:1100–1107.
33. Nikolaev P, et al. (2016) Autonomy in materials research: A case study in carbon nanotube growth. *NPJ Comp Mater* 2:16031.
34. Nikolaev P, Hooper D, Perea-López N, Terrones M, Maruyama B (2014) Discovery of wall-selective carbon nanotube growth conditions via automated experimentation. *ACS Nano* 8:10214–10222.
35. Jang J, Schatz GC, Ratner MA (2003) Capillary force on a nanoscale tip in dip-pen nanolithography. *Phys Rev Lett* 90:156104–156107.
36. Giam LR, et al. (2012) Scanning probe-enabled nanocombinatorics define the relationship between fibronectin feature size and stem cell fate. *Proc Natl Acad Sci USA* 109:4377–4382.
37. Fahrni CJ (2007) Biological applications of X-ray fluorescence microscopy: Exploring the subcellular topography and speciation of transition metals. *Curr Opin Chem Biol* 11:121–127.
38. Yang F, et al. (2014) Chirality-specific growth of single-walled carbon nanotubes on solid alloy catalysts. *Nature* 510:522–524.
39. Guisbiers G, et al. (2014) Gold-copper nano-alloy, "tumbaga," in the era of nano: Phase diagram and segregation. *Nano Lett* 14:6718–6726.
40. Takagi D, Homma Y, Hibino H, Suzuki S, Kobayashi Y (2006) Single-walled carbon nanotube growth from highly activated metal nanoparticles. *Nano Lett* 6:2642–2645.
41. Homma Y, Liu H, Takagi D, Kobayashi Y (2009) Single-walled carbon nanotube growth with non-iron-group "catalysts" by chemical vapor deposition. *Nano Res* 2:793–799.
42. Kim D, Resasco J, Yu Y, Asiri AM, Yang P (2014) Synergistic geometric and electronic effects for electrochemical reduction of carbon dioxide using gold-copper bimetallic nanoparticles. *Nat Commun* 5:4948.
43. Eichelsdoerfer DJ, et al. (2013) Large-area molecular patterning with polymer pen lithography. *Nat Protoc* 8:2548–2560.